AIP | Applied Physics Letters

Diffusion-limited kinetics of the antiferromagnetic to ferrimagnetic λ-transition in Fe1−xS

F. William Herbert, Aravind Krishnamoorthy, Bilge Yildiz, and Krystyn J. Van Vliet

Citation: Applied Physics Letters **106**, 092402 (2015); doi: 10.1063/1.4913201
View online: http://dx.doi.org/10.1063/1.4913201
View Table of Contents: http://scitation.aip.org/content/aip/journal/apl/106/9?ver=pdfcov
Published by the AIP Publishing

Diffusion-limited kinetics of the antiferromagnetic to ferrimagnetic λ-transition in $Fe_{1-x}S$

F. William Herbert,[1,2,3] Aravind Krishnamoorthy,[1,2] Bilge Yildiz,[1,2,4,a)] and Krystyn J. Van Vliet[1,3,b)]
[1]*Department of Materials Science and Engineering, Massachusetts Institute of Technology, Cambridge, Massachusetts 02139, USA*
[2]*Laboratory for Electrochemical Interfaces, Massachusetts Institute of Technology, Cambridge, Massachusetts 02139, USA*
[3]*Laboratory for Material Chemomechanics, Massachusetts Institute of Technology, Cambridge, Massachusetts 02139, USA*
[4]*Department of Nuclear Science and Engineering, Massachusetts Institute of Technology, Cambridge, Massachusetts 02139, USA*

(Received 19 November 2014; accepted 3 February 2015; published online 2 March 2015)

$Fe_{1-x}S$ ($0.08 \leq x \leq 0.11$) exhibits a simultaneous magneto-structural "λ-transition" at approximately 200 °C. Time-dependent magnetization measurements demonstrate the λ-transition can be accurately modeled by a stretched exponential function, consistent with a nucleation-free, continuous reordering of the vacancy-bearing sublattice. The experimental result is supported by kinetic Monte Carlo simulations that confirm the activation energy for the transition to be 1.1 ± 0.1 eV—representing the iron vacancy migration energy in ordered $Fe_{1-x}S$. A mechanistic understanding of the λ-transition enables potential functional uses of $Fe_{1-x}S$ such as thermally activated magnetic memory, switches, or storage. © *2015 AIP Publishing LLC*. [http://dx.doi.org/10.1063/1.4913201]

Pyrrhotites are a set of cation-deficient iron monosulfides across the narrow composition range $0 \leq x \leq 0.125$ in $Fe_{1-x}S$. The unusual magnetic properties of pyrrhotite have long been studied for their fundamental interest. Recently, $Fe_{1-x}S$ nanowires[1,2] and nanodisks[3] that display an antiferromagnetic (AF) to ferrimagnetic (FI) "λ-transition" upon heating have been investigated and proposed for technological purposes such as phase-change magnetic memory devices.[4] $Fe_{1-x}S$ is known to display independent ferroelectric[5] and local ferromagnetic properties, depending on composition, suggesting it may be a candidate single-phase multiferroic material,[6] similar to NiS,[7] $CuCrS_2$,[8] and $AgCrS_2$.[9] In this regard, $Fe_{1-x}S$ presents a low cost, non-toxic, and earth-abundant option. However, there remains considerable confusion regarding the mechanisms of the magnetic transitions in pyrrhotite, including the origin of the λ-transition. Prior attempts to quantify the AF-FI transformation kinetics assumed simple, exponential kinetics that fail to capture adequately the underlying atomic-scale lattice rearrangements.[10,11]

First, we briefly review the atomic scale structural changes associated with the λ-transition, aided by the phase diagram in Figure 1(a). The basic unit cell for all $Fe_{1-x}S$ compositions is NiAs-type hexagonal with the space group $P6\bar{2}c$. Below a common magnetic ordering (Néel) temperature T_N of 320 °C, $Fe_{1-x}S$ forms a series of complex, structurally ordered polytypes based on Kagome nets, minimizing total vacancy-vacancy interaction energy.[12] The superstructures are defined by a periodicity of full- and partially vacant Fe atom layers, stacked along the *c*-axis. In-plane, Fe atoms are aligned ferromagnetically (↑ ↑ ↑ ↑), whereas AF (↓ ↑ ↓ ↑) coupling arises between adjacent layers.[11] The presence of iron vacancies on any given *a-b* plane reduces the overall ferromagnetic moment; net magnetism is hence determined by the symmetry of layer occupancy. For example, "4C" pyrrhotite ($Fe_{1-x}S$; $x = 0.125 \pm 0.05$) adopts a monoclinic structure in which the cation layers alternate between full and quarter-vacant, resulting in net ferrimagnetism (Fig. 1(b)).[13] In the composition range $0.08 \leq x \leq 0.11$, on the other hand, $Fe_{1-x}S$ forms a set of AF, hexagonal superstructures known collectively as "NC," $5 \leq N \leq 11$ (e.g., Fig. 1(c)[14]). The temperature-dependent magnetization $\sigma(T)$ of AF, NC-ordered pyrrhotites is characterized by the appearance of a peak during heating, centered around 210 °C, believed to arise from a diffusive structural rearrangement towards an FI superlattice (λ-transition).[15]

An initial attempt to replicate the earlier kinetic experiments of Marusak *et al.*[11] revealed a more complex time-evolution of the ferrimagnetic superlattice than previously appreciated. Instead of a simple exponential fit, we demonstrate the magnetokinetics are better modeled by a phenomenological, stretched exponential function of the form

$$\alpha(t) = 1 - \exp\left[-(t/\tau)^n\right], \quad (1)$$

where τ describes a temperature-dependent relaxation time, and $n = 0.45 \pm 0.05$. Moreover, we conducted kinetic Monte Carlo (kMC) simulations of the λ-transition that reproduced the structural evolution on the experimental timescale from an AF to FI lattice under cation vacancy diffusion alone. The kMC results similarly give a stretched exponential time dependence and help understand the transition as a continuous-ordering transformation. A physical basis for the stretched exponential form of the kinetics is discussed. Finally, we show the temperature dependence of τ in Eq. (1) yields an activation energy of 1.1 ± 0.1 eV for the λ-transition, which can be taken as the migration energy for cation diffusion in ordered pyrrhotite.

a)Electronic mail: byildiz@mit.edu
b)Electronic mail: krystyn@mit.edu

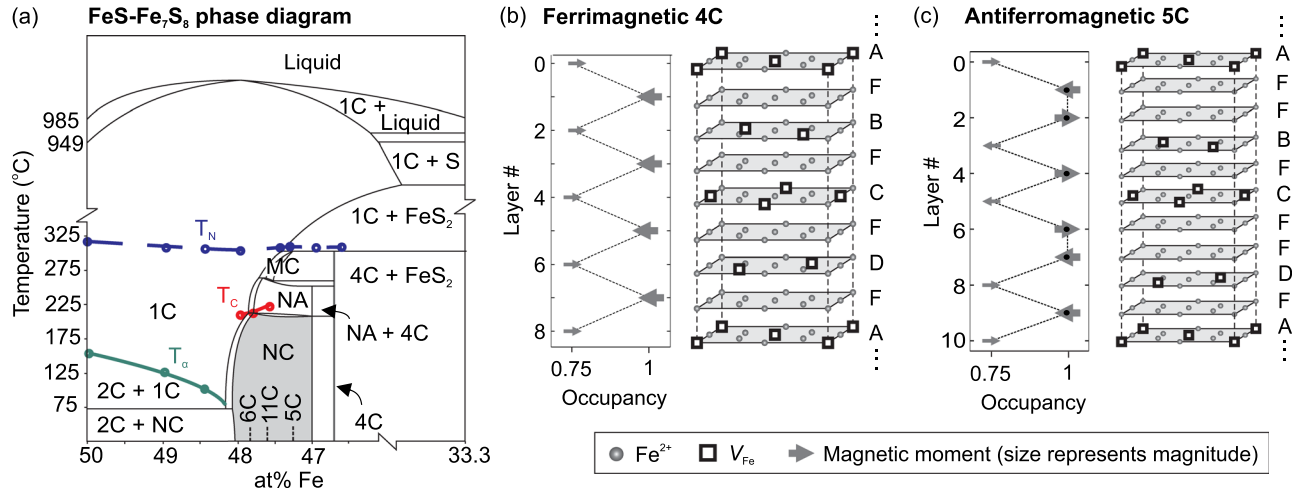

FIG. 1. (a) Fe-S phase diagram in the composition range $0 \le x \le 0.125$ in $Fe_{1-x}S$, showing the existence range of the different pyrrhotite polytypes.[14] Experimentally determined temperatures for the α-, β– and λ–transition onsets (T_α, T_N, and T_C, respectively) are also shown.[16–18] (b) Equilibrium $Fe_{1-x}S$ 4C superstructure with alternating full and partially vacant occupancy of *AB*-layers. An uncompensated magnetic moment results in net ferrimagnetism. "F" refers to full Fe layers; A–D are vacancy-bearing layers with different in-plane vacancy arrangements. (b) Idealized 5C superstructure with net magnetic compensation between full and vacancy-bearing layers; net antiferromagnetism.

Fe_7S_8 (4C), $Fe_{10}S_{11}$ (11C), and $Fe_{11}S_{12}$ (6C) pyrrhotite samples were prepared by reacting the requisite amounts of high-purity iron and sulfur powders in vacuum-sealed quartz tubes.[14] Magnetic measurements were obtained using a variable-temperature Vibrating Sample Magnetometer (VSM) under a flowing N_2 atmosphere and an applied field of 10 kOe.

Temperature-dependent magnetization $\sigma(T)$ results for the 4C, 11C, and 6C $Fe_{1-x}S$ samples are shown in Figure 2. The 4C pyrrhotite followed reversible FI, Weiss-type behavior as expected up to $T_N = 320\,^\circ C$ (Fig. 2(a)). However, the 11C and 6C displayed markedly different $\sigma(T)$ behavior (Figs. 2(b) and 2(c)). On the first heating cycle, labelled (1) in the figures, σ started close to 0 emu/g, consistent with AF ordering. The λ-transition peak[10,11] was observed starting around 180 °C, with a maximum at 210 °C. However, during the cooling portion of the cycle from 350 °C, the peak was not reproduced and σ increased with Weiss behavior back to room temperature. Multiple, repeated heating/cooling cycles (2–5) as indicated on the curves only served to increase overall magnitization further. The maximum room temperature magnetization σ_{RT} reached by 11C after several experimental cycles (~13 emu/g) was greater than that of the 6C sample (~10 emu/g); neither reached the maximum of the 4C sample ($\sigma_{RT} \sim 22$ emu/g). Thus, the final σ for a given structure is limited by the availability of iron vacancies V_{Fe} to maximize the magnetic asymmetry between vacancy-bearing and full layers.

To understand the transformation kinetics in more detail, we performed isothermal, $\sigma(t)$ measurements on samples of 11C between 140–220 °C. Assuming V_{Fe} diffusion-driven exponential growth in σ during the λ-transition, iron self-diffusion coefficients on the order of $10^{-17}\,cm^2\,s^{-1}$ have been found by magnetokinetic methods within this transition temperature range[11] that are inconsistently low compared to extrapolated diffusivities obtained from high-temperature sulfidation[19,20] and radiotracer diffusion studies [$O(10^{-14}\,cm^2\,s^{-1})$].[21] However, we found that our magnetokinetic data were more accurately described by the stretched exponential function in Eq. (1).[14]

We first converted experimental σ to "phase fraction" of FI ordering, α_{FI}, according to

$$\alpha_{FI} = \frac{(\sigma_t - \sigma_i)}{(\sigma_f - \sigma_i)}, \tag{2}$$

where σ_t is the measured magnetization at time t, σ_i is initial magnetization at $t = 0$, and σ_f is final magnetization assuming the transition were allowed to proceed to completion. σ_f values for the different temperatures were therefore obtained

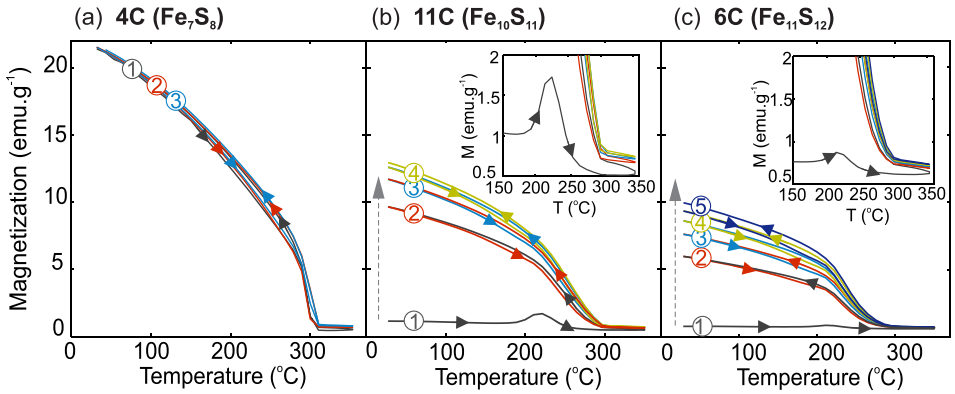

FIG. 2. Temperature-dependent magnetization $\sigma(T)$ for: (a) 4C, (b) 11C, and (c) 6C pyrrhotite samples. Multiple consecutive forward and reverse sweeps between 30 and 330 °C, as labelled 1–5 on each of the graphs, were performed until no change from the previous sweep was observed. On (b) and (c) the inset graphs show a magnified region around the peak observed on the first sweep. The heating and cooling rates were both 0.2 °C/min; the applied field was 10 kOe.

from curve number (4) in Fig. 2(b), i.e., the maximum FI magnetization.

The experimental data were complemented by kMC simulations (full details in Ref. 14), based on the probability P of a diffusive vacancy jump, given by: (i) the intrinsic activation barrier to migration E_m; (ii) an energy bias, E_{therm}, due to a thermodynamic driving force towards ordering; and (iii) a bias due to the magnetic energy, E_{mag}

$$P = \nu . \exp\left[-\frac{E_m}{k_B T}\right] \exp\left[-\frac{E_{therm}}{k_B T}\right] \exp\left[-\frac{E_{mag}}{k_B T}\right], \quad (3)$$

where k_B is Boltzmann's constant. The energy barrier E_m was taken to be 1.2 eV, as calculated from Density Functional Theory.[14] The energy term E_{therm} was based on thermodynamic data for pyrrhotite polytypes.[22] Subsequent to each diffusive jump, an order parameter Θ was assigned to the updated structure, based on the root mean squared (RMS) difference from the periodically alternating occupancy of a perfectly vacancy-segregated superstructure. Net magnetization σ was evaluated by summing over all individual magnetic moments on lattice sites.

Figures 3(a) and 3(b) show the results for the experimental and simulated λ-transition magnetokinetics, with $n = 0.45 \pm 0.05$ and 0.67 ± 0.05, respectively (sensitivity analysis in Ref. 14). Nevertheless, the kMC model, based solely on cation diffusion, accurately replicates the stretched exponential form of the experimental results. The parameters τ in Eq. (1) generally represents a temperature-dependent relaxation time and n describes the deceleration in transition kinetics as it progresses. Stretched exponential magnetokinetics have been observed for $Li_2(Li_{1-x}Fe_x)N$ due to non-instantaneous magnetic moment relaxation,[23] unlikely at the elevated temperatures used in this work. Alternatively, we can consider the λ-transition as a classical nucleation and growth process, described by the semi-empirical Johnson-Mehl-Avrami-Kolmogorov (JMAK) relation that takes the same form as Eq. (1). For example, the antiferromagnetic-ferromagnetic transition in FeRh has been described by a JMAK equation with $n = 0.86$.[24] The Avrami exponent n may provide information about the nucleation and growth mechanisms.[25] However, we believe the microscopic transition mechanism can be better described as a diffusion-limited, continuous re-ordering process akin to spinodal decomposition. As such, the FI phase grows out of the AF lattice via an augmentation in small, layer-by-layer vacancy occupancy fluctuations. A second-order transition of this type is consistent with a continuity in enthalpy H but discontinuous heat capacity $\partial H/\partial T$ during the λ-transition, as measured by DSC.[14]

Recalling the interdependence between the vacancy and magnetic structures, the simulation results thus visualize the emergence of diffuse regions of intermediate Θ that gradually spread across other lattice points in diffuse zones rather than the formation of discrete FI nuclei (Figs. 4(a)–4(e)), also seen in Figure 4(f), where small fluctuations in layer-by-layer vacancy occupancy augment with time into an alternating-plane, FI structure.

The stretched exponential fits of Eq. (1) to our measured and calculated $\sigma(t)$ take the same form as the Kohlrausch (or

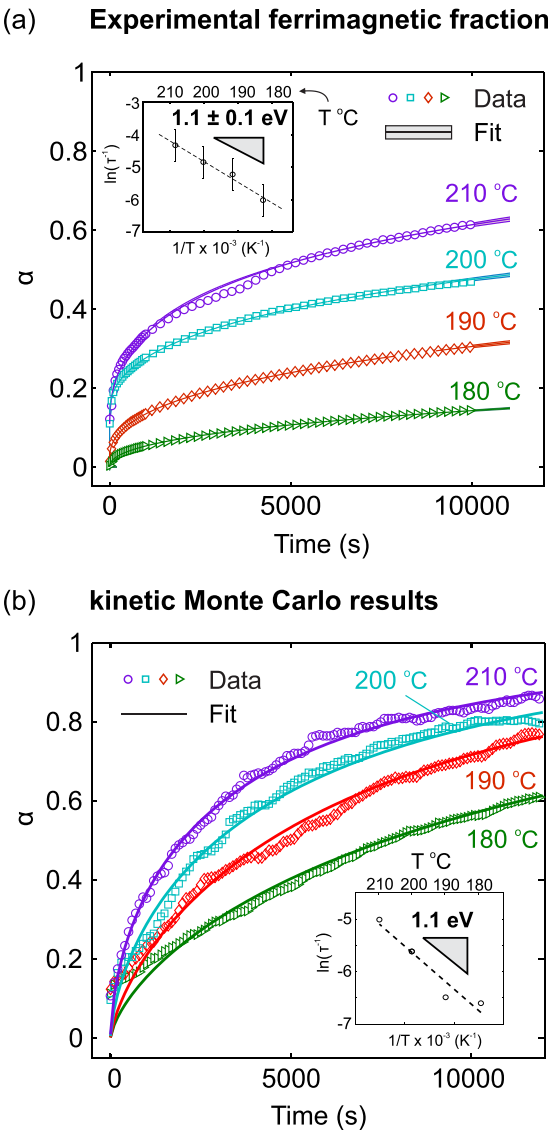

FIG. 3. (a) Transformed ferrimagnetic volume fraction α measured over 10 000 s at four temperatures as indicated. We show every twentieth point of the raw data, as well as a best fit line to the phenomenological, stretched exponential relation $\alpha(t) = 1 - \exp[-(t/\tau)^n]$, with error represented as standard deviation. Inset: Arrhenius fit of the temperature-dependent fitting parameter τ^{-1}, with a slope corresponding to a transformation activation energy of 1.1 ± 0.1 eV. (b) kMC reullts for magnetization transformation at the same temperatures, and fit to a similar stretched exponential fit. Inset: corresponding activation energy of 1.1 eV calculated from computational τ^{-1}.

KWW) function,[26] commonly used to describe non-equilibrium dynamics in disordered condensed matter[27,28] and diffusion in complex systems.[29] Although generically semi-empirical, we may draw some parallels with mathematical derivations for the Kohlrausch function[30] to suggest a more physical basis for the observed behavior. For example, a small energy distribution of energy traps may lead to deviations from "random walk" Brownian motion diffusion. Alternatively, there may be a time-dependence in populating different traps, such that relaxation occurs in stages.[31] We dismiss the former since Brownian motion was inherently assumed in our kMC model. On the other hand, a time-decay in the rate of magnetization evolution may be more coherently explained by a combination of rapid and subordinate, slower processes. In other words, given sufficient thermal

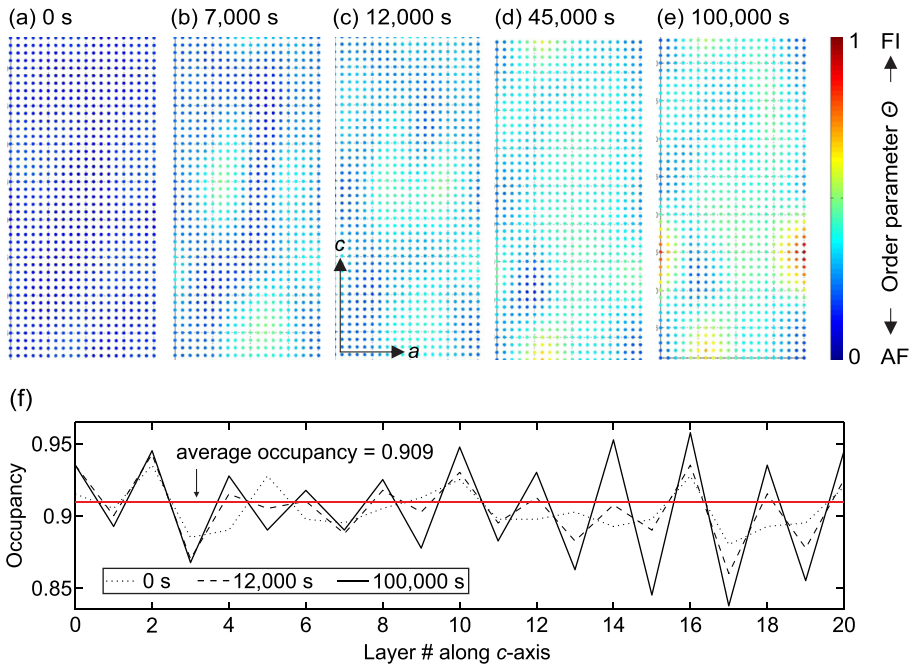

FIG. 4. Local order parameter Θ calculated for individual lattice points in the kMC simulation, where 0 refers to fully antiferromagnetic (AF) and 1 is ferrimagnetic (FI), corresponding to: (a) 0 s, (b) 7000 s, (c) 12 000 s, (d) 45 000 s, and (e) 100 000 s hold times at 200 °C. (f) Layer-by-layer occupancy for 20 planes along the *c*-axis from the kMC results obtained at different times. As the transition progresses, the difference in occupation between adjacent layers becomes more pronounced.

energy cation vacancies may migrate rapidly to adjacent planes under a large thermodynamic driving force and break the magnetically compensating AF lattice symmetry. Small regions with localized FI ordering would nonetheless contribute a large increase in σ on the scale of 10–100 s of seconds. At longer times, however, the formation of the optimal FI lattice structure for the available vacancy concentration requires a more labored rearrangement of vacancies into long-range order, slowing down the growth in σ. Only out-of-plane V_{Fe} hops contribute to a rise in magnetization; however, in-plane hops continue to occur and would contribute to the lengthening of the relaxation time. We compared the ratio of out-of-plane to in-plane hops during the λ-transition in our kMC model and found that it decreased over time. Due to vacancy repulsion effects, the further the transition progresses, the lower the driving force for vacancy segregation and the smaller the probability of out-of-plane jumps.

Finally, we turn to the significance of the activation energy of 1.1 ± 0.1 eV measured by fitting the experimental $\sigma(t)$. A migration barrier for diffusion of 1.2 eV was originally cast into our kMC model based on DFT calculations. An analysis of the resulting kMC data using the same fitting procedure as for the experiment returned an apparent barrier value of 1.1 eV, confirming that the major rate-limiting step is cation diffusion. The measured activation energy includes a thermodynamic bias for the transformation on the order of 0.1 eV at 200 °C, which lowers the diffusion barrier slightly.

In conclusion, we have investigated the antiferromagnetic to ferrimagnetic λ-transition in NC-type pyrrhotites via magnetokinetic experiments and kinetic Monte Carlo simulations. In contrast to previous reports, the transformation follows a stretched exponential time-dependence. These experimental and computational results together support a description of the λ-transition as a nucleation-free, continuous reordering via diffusion on the cation sublattice. Magnetization initially rises rapidly due to small, localized displacements, but a full optimization of the ferrimagnetic superstructure is a more complex process that emerges only at longer timescales. The migration energy barrier for Fe in magnetic pyrrhotite is confirmed to be approximately 1.1 eV. The elucidation of the kinetics for this λ-transition stimulates continued studies of the rate-limiting steps of this interesting magnetic transition and the consideration of synthetic $Fe_{1-x}S$ in multiferroic systems, magnetic switching, or data recording devices enabled by earth-abundant elements.

We gratefully acknowledge the support provided by BP Plc. through the BP-MIT center for Materials and Corrosion Research. We also thank David Bono, Dr. Nicolas Aimon, and Max Brosnahan for assistance with vibrating sample magnetometer experiments. We thank NSF for computational resources provided through the Texas Advanced Computing Center under Grant No. TG-DMR120025.

[1]G. H. Yue, P. X. Yan, X. Y. Fan, M. X. Wang, D. M. Qu, D. Yan, and J. Z. Liu, "Characterization of the single crystalline iron sulfide nanowire array synthesis by pulsed electrodeposition," J. Appl. Phys. **100**(12), 124313 (2006).
[2]M. Nath, A. Choudhury, A. Kundu, and C. N. R. Rao, "Synthesis and characterization of magnetic iron sulfide nanowires," Adv. Mater. **15**(24), 2098–2101 (2003).
[3]I. S. Lyubutin, C.-R. Lin, S.-Z. Lu, Y.-J. Siao, Y. V. Korzhetskiy, T. V. Dmitrieva, Y. L. Dubinskaya, V. S. Pokatilov, and A. O. Konovalova, "High-temperature redistribution of cation vacancies and irreversible magnetic transitions in $Fe_{1-x}S$ nanodisks observed by Mössbauer spectroscopy and magnetic measurements," J. Nanopart. Res. **13**(10), 5507–5517 (2011).
[4]T. Takayama and H. Takagi, "Phase-change magnetic memory effect in cation-deficient iron sulfide $Fe_{1-x}S$," Appl. Phys. Lett. **88**(1), 012512 (2006).
[5]F. Li, H. F. Franzen, and M. J. Kramer, "Ordering, incommensuration, and phase transitions in pyrrhotite: Part I: A TEM study of Fe_7S_8," J. Solid State Chem. **124**(2), 264–271 (1996).
[6]W. Eerenstein, N. D. Mathur, and J. F. Scott, "Multiferroic and magnetoelectric materials," Nature **442**, 759–765 (2006).
[7]A. Mandala, A. Bosea, S. Mitraa, A. Dattac, S. Banerjeeb, and D. Chakravortya, "Multiferroic properties of NiS nanoplates grown within Na-4 mica," J. Magn. Magn. Mater. **324**, 2861 (2012).

[8]A. Karmakar, K. Dey, S. Chatterjee, S. Majumdar, and S. Giri, "Spin correlated dielectric memory and rejuvenation in multiferroic $CuCrS_2$," Appl. Phys. Lett. **104**, 052906 (2014).
[9]F. Damay, C. Martin, V. Hardy, G. Andre, S. Petit, and A. Maignan, "Magnetoelastic coupling and unconventional magnetic ordering in the multiferroic triangular lattice $AgCrS_2$," Phys. Rev. B **83**, 184413 (2011).
[10]M. G. Townsend, A. H. Webster, J. L. Horwood, and H. Roux-Buisson, "Ferrimagnetic transition in $Fe_{0.9}S$: Magnetic, thermodynamic and kinetic aspects," J. Phys. Chem. Solids **40**(3), 183–189 (1979).
[11]L. A. Marusak and L. N. Mulay, "Polytypism in the cation-deficient iron sulfide, Fe_9S_{10}, and the magnetokinetics of the diffusion process at temperatures about the antiferro- to ferrimagnetic λ phase transition," Phys. Rev. B **21**, 238–244 (1980).
[12]I. S. Hagemann, Q. Huang, X. P. A. Gao, A. P. Ramirez, and R. J. Cava, "Geometric magnetic frustration in a two-dimensional spinel based Kagomé lattice," Phys. Rev. Lett. **86**(5), 894–897 (2001).
[13]A. V. Powell, P. Vaqueiro, K. S. Knight, L. C. Chapon, and R. D. Sánchez, "Structure and magnetism in synthetic pyrrhotite Fe_7S_8: A powder neutron-diffraction study," Phys. Rev. B **70**, 014415 (2004).
[14]See supplementary material at http://dx.doi.org/10.1063/1.4913201 for further details on pyrrhotite polytypes, sample preparation, kinetic Monte Carlo simulations, density functional theory calculations, short-timescale magnetization results, differential scanning calorimetry, and fitting parameters.
[15]F. K. Lotgering, "Ferrimagnetism of sulfides and oxides," Phillips Res. Rep. **11**, 190–217 (1956).
[16]S. A. Kissin and S. D. Scott, "Phase relations involving pyrrhotite below 350 °C," Economic Geology **77**(7), 1739–1754 (1982).
[17]H. Nakazawa and N. Morimoto, "Phase relations and superstructures of pyrrhotite, $Fe_{1-x}S$," Mater. Res. Bull. **6**(5), 345–357 (1971).
[18]E. J. Schwarz and D. J. Vaughan, "Magnetic phase relations of pyrrhotite," J. Geomagn. Geoelectr. **24**(4), 441–458 (1972).
[19]M. Danielewski, S. Mrowec, and A. Stoaosa, "Sulfidation of iron at high temperatures and diffusion kinetics in ferrous sulfide," Oxid. Met. **17**(1–2), 77–97 (1982).
[20]E. M. Fryt, W. W. Smeltzer, and J. S. Kirkaldy, "Chemical diffusion and point defect properties of iron sulfide at temperatures 600 °C," J. Electrochem. Soc. **126**(4), 673–683 (1979).
[21]R. H. Condit, R. R. Hobbins, and C. E. Birchenall, "Self-diffusion of iron and sulfur in ferrous sulfide," Oxid. Met. **8**(6), 409–455 (1974).
[22]P. Walder and A. D. Pelton, "Thermodynamic modeling of the Fe-S system," J. Phase Equilib. Diffus. **26**(1), 23–38 (2005).
[23]A. Jesche, R. W. McCallum, S. Thimmaiah, J. L. Jacobs, V. Taufour, A. Kreyssig, R. S. Houk, S. L. Budanko, and P. C. Canfield, "Giant magnetic anisotropy and tunnelling of the magnetization in $Li_2(Li_{1-x}Fe_x)N$," Nat. Commun. **5**, 3333 (2014).
[24]M. Loving, "Understanding the magnetostructural transformation in FeRh thin films," Ph.D. dissertation (Northeastern University, 2014).
[25]R. W. Balluffi, S. M. Allen, and W. C. Carter, *Kinetics of Materials* (Wiley, 2005).
[26]R. Metzler and J. Klafter, "The random walk's guide to anomalous diffusion: a fractional dynamics approach," Phys. Rep. **339**(1), 1–77 (2000).
[27]A. K. Jonscher, "Dielectric relaxation in solids," J. Phys. D: Appl. Phys. **32**(14), R57 (1999).
[28]E. B. Walton and K. J. VanVliet, "Equilibration of experimentally determined protein structures for molecular dynamics simulation," Phys. Rev. E **74**(6), 061901 (2006).
[29]J. Kakalios, R. A. Street, and W. B. Jackson, "Stretched-exponential relaxation arising from dispersive diffusion of hydrogen in amorphous silicon," Phys. Rev. Lett. **59**(9), 1037–1040 (1987).
[30]J. Klafter and M. F. Shlesinger, "On the relationship among three theories of relaxation in disordered systems," Proc. Natl. Acad. Sci. **83**(4), 848–851 (1986).
[31]R. G. Palmer, D. L. Stein, E. Abrahams, and P. W. Anderson, "Models of hierarchically constrained dynamics for glassy relaxation," Phys. Rev. Lett. **53**(10), 958–961 (1984).